Chapter 3

Monolayer and Multilayer Films of Novel Ionic Mesogenic PyTp and DNA Complex at Interfaces

3.1 Introduction

The interaction of DNA with molecules in a monolayer at the air-water (A-W) interface has received considerable attention in recent years [1]. Several studies have been carried out with a view to understand templated supramolecular organization as well as the transfer of DNA across biological bilayer membranes [2–4]. A variety of cationic surfactants, like linear and branched polymer, glycopeptides, dendrimers as well as lipid membranes, have been shown to be capable of complexing with DNA [5, 6]. In particular, the cationic lipids complexed with DNA are promising nonviral carriers of DNA vectors for gene therapy [7]. Additionally, the lipid-DNA complexes find application in nucleic acid based biosensors. Langmuir-Blodgett (LB) films are useful for immobilization of nucleic acids (DNA, polynucleotides) by electrostatic interaction on solid supports in the designing of such biosensors [8]. The ability of double stranded DNA to act as a conduit for electron transfer over long range, and the corresponding inability of single stranded DNA to do the same, has been the basis for DNA hybridization biosensors [9]. The immobilization of DNA molecules on a solid substrate by means of electrostatic interaction has clear advantage compared to chemical bonding. These are not only the simplicity and accessibility of the immobilization technique, but also the possibility of using a variety of solid substrates with any optical, electrical, magnetic and mechanical properties.

Although there have been many studies on the formation of DNA-cationic lipid complexes, there have been no reports on the interaction of DNA with cationic discotic molecules at the A-W interface. Recently, Cui et. al. have reported DNA complexes with cationic discotic surfactants in the bulk, which have specific electronic and optical properties for potential applications such as one-dimensional semiconductors, nonlinear optics, field-effect transistors and photovoltaics [10]. The interaction of DNA with discotic surfactant in the bulk is different from such an interaction at the A-W interface. In the bulk, the discotic surfactants can interact on both sides of DNA, whereas at A-W interface, the discotic surfactants can interact only on those parts of DNA which are accessible at the interface. However, the nature of these interactions and the structure-property relationships of such discotic-DNA complexes have not yet been properly studied and understood.

In the previous chapter, we have discussed the formation of a stable monolayer of PyTp molecules at the A-W interface. An interesting aspect of the system is that the molecule PyTp is cationic. This provides opportunity to explore the possibilities of a complex formation between the PyTp molecule and negatively charged species like DNA. In this chapter, we show the formation of a stable complex between the PyTp monolayer and DNA at the A-W interface. We find that, compared to the pure PyTp monolayer, the PyTp-DNA complex monolayer exhibits higher collapse pressure indicating better stability. In addition, the PyTp-DNA complex monolayer does not revert from the collapsed state unlike that of pure PyTp monolayer. Atomic force microscope (AFM) studies show that the PyTp-DNA complex films transferred onto silicon substrates are quite compact. AFM has also been used to study the mechanical properties of film surfaces on the nanometer scale by nanoindentation [11]. We have used nanoindentation technique to study qualitatively the hardness of pure PyTp as well as PyTp-DNA complex films at nanometer scale. We find that the PyTp-DNA complex film is about two times harder than the pure PyTp film.

3.2 Experiment

The material, pyridinium salt tethered with hexaalkoxytriphenylene (PyTp) molecule with bromide counterion, was synthesized in the chemistry laboratory of our institute by Sandeep Kumar and Santanu Kumar Pal [12]. The details of the material PyTp are mentioned in Chapter 2. For

its complexation with DNA, sodium salts of deoxyribonucleic acid (from Salmon testes) was dissolved in the ultrapure water subphase. This is a double stranded DNA with approximate molecular weight of 1.3×10^6 and about 2000 base pair (Sigma). To check the purity of DNA, we have carried out UV-visible spectroscopy. For pure DNA, the maximum absorption occurs at about 260 nm. The protein molecules, which are a frequent contaminant of DNA preparation, absorb at 280 nm. We found no absorption band at 280 nm in the UV-visible spectrum of DNA. This indicates that the DNA which we have used in our experiments was very pure without any contamination of proteins.

The surface pressure (π) - area per molecule (A_m) isotherm for the complex monolayer was obtained by spreading 0.236 mM concentration solution of PyTp in chloroform (HPLC grade) on the subphase containing DNA at various concentrations. The surface pressure measurements with time were carried out to investigate the stability of the PyTp-DNA complex monolayer. Brewster angle microscope (BAM) was used for in situ observation of the morphology of the complex film at the A-W interface. In addition, reflection microscope was used to observe three-dimensional (3D) collapse domains of the films at the A-W interface. LB technique was employed to transfer films of PyTp-DNA complex onto hydrophilic and hydrophobic silicon substrates at different target surface pressures (π_t). The hydrophilic and hydrophobic substrate preparation methods are mentioned in the Experiment section of Chapter 2.

The LB films were studied using AC mode AFM in ambient condition. To determine the thickness of compact films, we have first scanned the film surface in AC mode AFM and obtained the topography image. Next, with the same tip, we have scratched the film in the contact mode and then imaged the scratched area in AC mode. The height profile across the scratch on the film gave the film thickness.

AFM was also used for nanoindentation to study the hardness of the pure film and complex film qualitatively. In this technique, AFM was used as a depth sensing instrument. Here, the cantilever deflection gives the load applied by the tip on the sample surface and the relative motion between the tip and the sample gives the indentation. AFM can provide versatile load range, obtained by changing the cantilever stiffness, which can vary between fractions of a nanoNewton upto a few

tens of a microNewton. The amount of deformation depends on the load applied. The deformations, that recover in the time scale of measurement, are generally taken to be elastic deformations and those which do not recover, are taken to be plastic deformation [13]. The advantage of using AFM as a nanoindenter was that we could observe the deformation (elastic or plastic) by imaging the area before and after indentation. Silicon tips of spring constant k_c of 5 N/m, and resonant frequency of 160 kHz were used. All measurements were carried out inside an environmental chamber in which dry nitrogen gas was circulated to avoid capillary condensation of water at the contact point between the tip and the surface.

Transmission Fourier transform infrared (FTIR) spectroscopy (Shimadzu 8400 FTIR) was carried out on these LB films to confirm the presence of DNA. All the experiments were carried out at room temperature (~25°C). The details of surface manometry, BAM and AFM are described in Chapter 1.

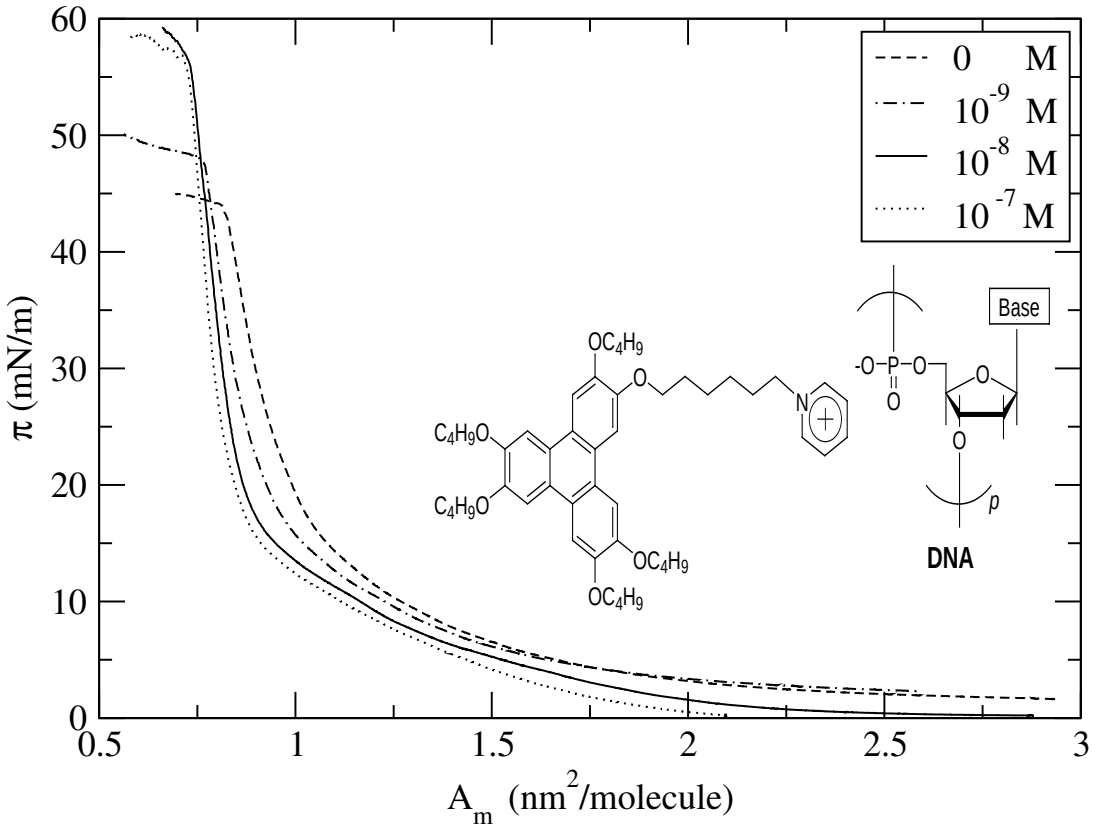

Figure 3.1: Surface pressure (π) - area per molecule (A_m) isotherms of PyTp-DNA complex monolayer for different concentrations of DNA in the subphase.

3.3 Results

3.3.1 Surface Manometry

The surface pressure (π) - area per molecule (A_m) isotherms for the PyTp molecule with different molar concentrations of DNA in the subphase are shown in Figure 3.1. We find that the collapse pressure (π_c) increases and the limiting area per molecule (A_o) of the isotherms decreases with the increase in the concentration of DNA in the subphase. However, beyond 10^{-8} M concentration of DNA, there was no further change in the isotherm. For the 10^{-8} M concentration, the collapse pressure was about 58 mN/m which is about 25% higher compared to the pure PyTp monolayer. The isotherm exhibited a clear slope change at 0.95 nm^2/molecule indicating a phase transformation. We find that 10^{-8} M is the optimum concentration of DNA in the subphase which is required to form a stable complex of PyTp-DNA at the A-W interface [14].

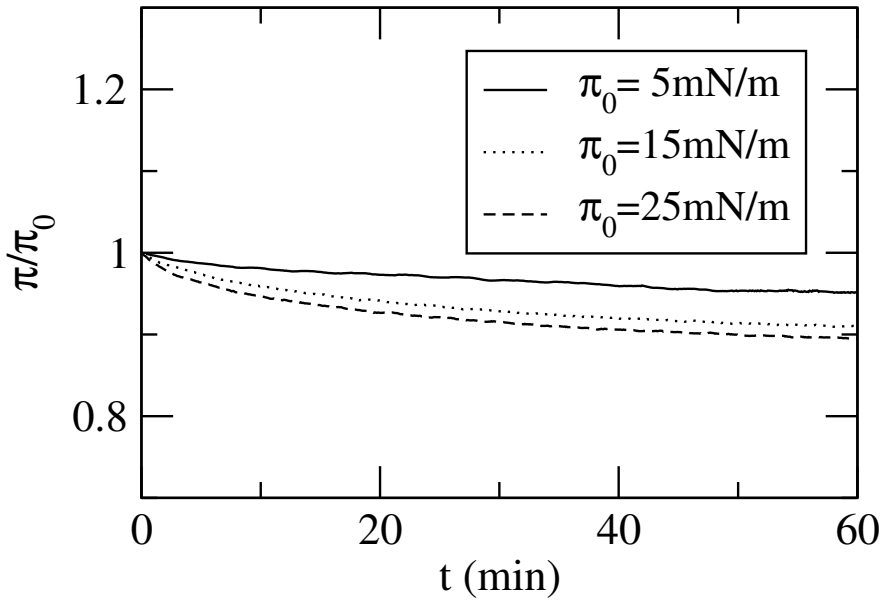

Figure 3.2: Surface pressure (π) - time (t) relaxation isotherms (normalized to π/π_0) of PyTp-DNA complex monolayer at constant area for various surface pressures (π_0).

The isocycles performed by compression and expansion of the PyTp-DNA complex monolayer at the condensed phase showed negligible amount of hysteresis. However, if the isocycles were performed after the complex monolayer reached the collapsed state, an appreciable amount of hysteresis was observed. Here, the monolayer did not exhibit reversibility on expansion. The surface pressure measurements with time (t) were carried out to further investigate the stability

of the PyTp-DNA complex monolayer with 10^{-8} M concentration of DNA in the subphase. The complex monolayer was compressed to a particular surface pressure (π_0), after which the surface pressure was recorded as a function of time at constant area. The π-t decay curves (normalized to π/π_0) of the PyTp-DNA complex monolayer obtained at constant area for different π_0 values, are shown in Figure 3.2. It was observed that the surface pressure was held quite stable over a large interval of time.

The compressional elastic modulus ($|E|$) was calculated using the expression,

$$|E| = A_m\left(\frac{d\pi}{dA_m}\right) \tag{3.1}$$

where $d\pi/dA_m$ is the change in surface pressure with area per molecule. The variation of $|E|$ with A_m obtained from the isotherms of pure PyTp monolayer, and PyTp-DNA complex monolayer with $10^{-8}M$ concentration of DNA in the subphase are shown in Figure 3.3. The $|E|$ value showed a maximum of 283 mN/m at A_m of 0.78 nm^2/molecule for the PyTp-DNA complex monolayer. This value is more than 3 times higher than the maximum $|E|$ value for the pure PyTp monolayer (83 mN/m).

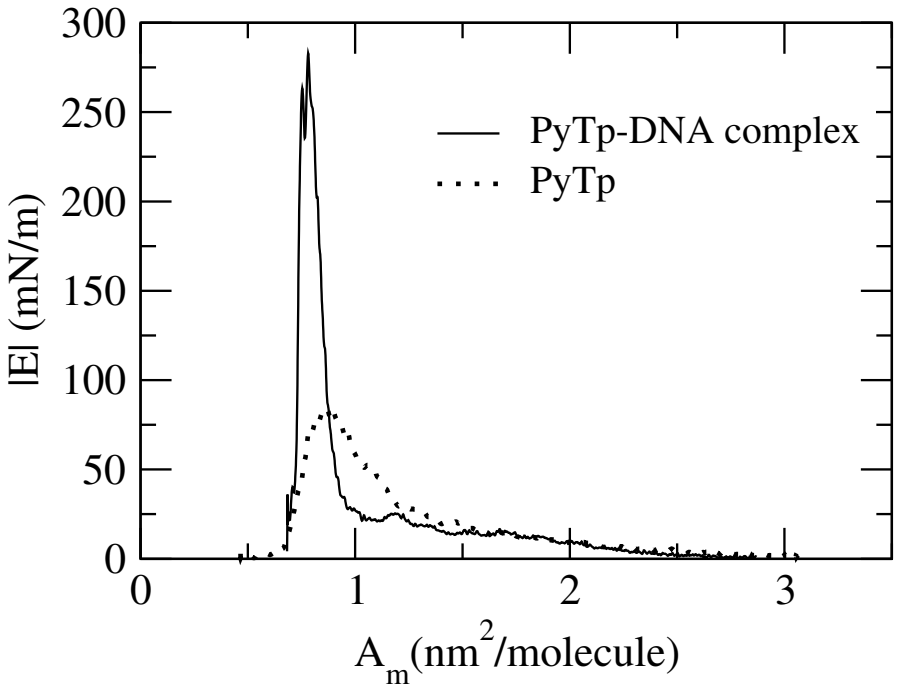

Figure 3.3: Variation of compressional elastic modulus ($|E|$) with area per molecule (A_m) for the pure PyTp monolayer, and the PyTp-DNA complex monolayer with $10^{-8}M$ concentration of DNA in the subphase.

3.3.2 Brewster Angle Microscopy

The BAM images of the PyTp-DNA complex monolayer with 10^{-8}M concentration of DNA in the subphase are shown in Figure 3.4. Similar to the pure PyTp monolayer, the intensity in the BAM image increases gradually upon compression (Figure 3.4(a)). But in the collapsed state, the 3D domains were markedly different. Pure PyTp film showed small crystalline domains filling the whole surface of water in a mesh-like texture (Chapter 2). On the contrary, the PyTp-DNA complex film showed long thread-like 3D domains (Figures 3.4(b) and 3.4(c)) at collapse. On expansion, these thread-like domains continued without change and the monolayer did not revert back to its original state. In addition, the collapsed state of these films were observed under reflection microscope. We find that the collapsed domains for the pure PyTp film were not resolved (Figure 3.5(a)) under reflection, whereas the thread-like collapse domains of PyTp-DNA complex film were clearly visible (Figure 3.5(b)).

3.3.3 Atomic Force Microscopy

3.3.3.1 Topography

For AFM studies, we have transferred the PyTp-DNA complex film (formed with 10^{-8} M concentration of DNA in the subphase) by LB technique onto both hydrophilic and hydrophobic silicon substrates. If the substrate is hydrophilic, the first monolayer is transferred as the substrate is raised through the subphase and subsequently a monolayer is deposited on each traversal of the substrate. Thus, a multilayer structure containing only an odd number of layers can be produced. However, if the substrate is hydrophobic, a monolayer will be deposited as it is first lowered into the subphase followed by successive deposition of layers on each stroke. This leads to a multilayer film structure containing an even number of layers [15]. We have prepared films containing odd number of layers on hydrophilic silicon substrates and films containing even number of layers on hydrophobic silicon substrates. For both the type of substrates, the transfer efficiency was close to unity.

AFM images of the PyTp-DNA complex monolayer transferred onto hydrophilic silicon substrates are shown in Figure 3.6. The film transferred at a π_t of 5 mN/m (Figure 3.6(a)) showed a

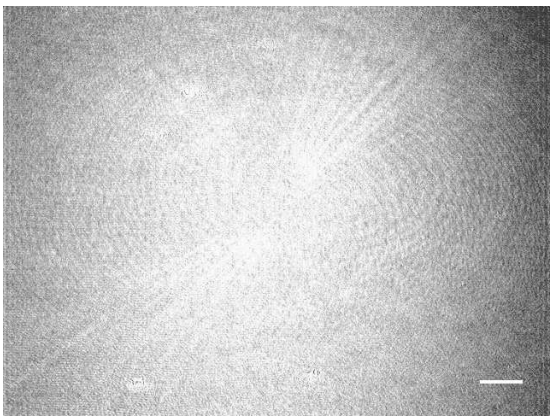

(a) $A_m = 0.85\ nm^2$

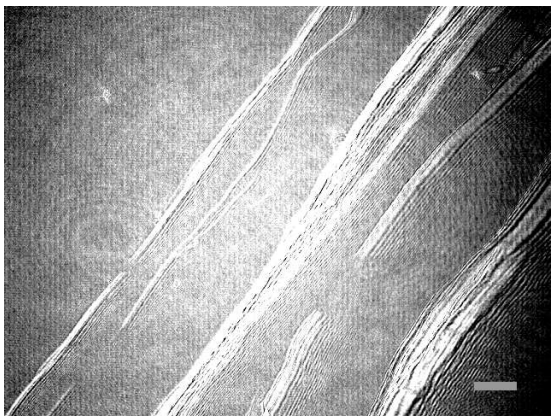

(b) $A_m = 0.55\ nm^2$

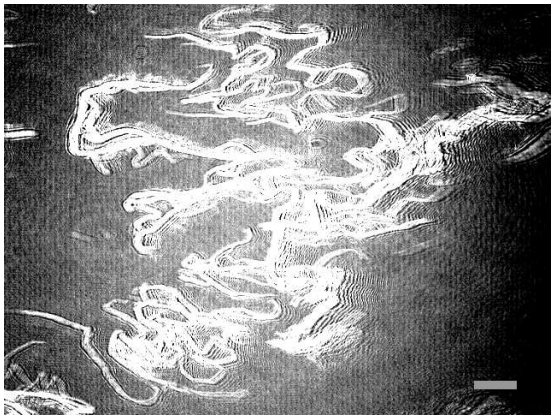

(c) $A_m = 0.35\ nm^2$

Figure 3.4: Brewster angle microscope images of PyTp-DNA complex monolayer at different area per molecule (A_m) with $10^{-8}M$ concentration DNA in the subphase. (a) Condensed phase. (b) and (c) Collapsed state with thread-like 3D crystalline domains. The scale bar in each image represents 500 μm.

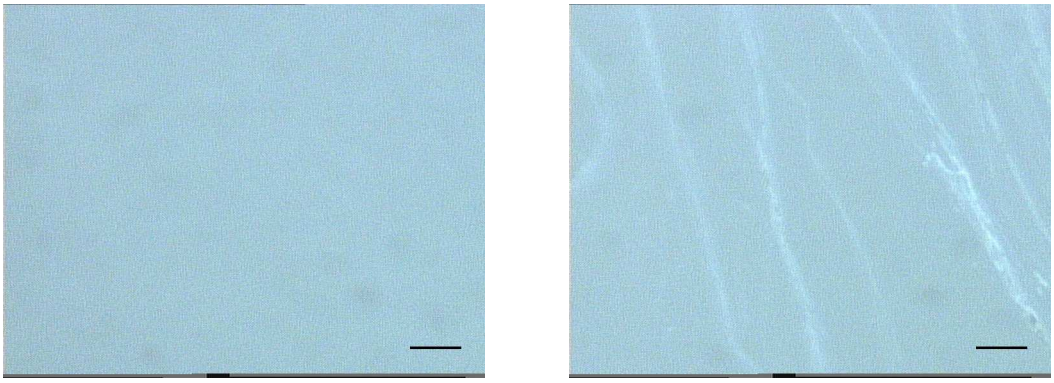

(a) (b)

Figure 3.5: Reflection microscope images obtained at the air-water interface for the collapsed state of (a) pure PyTp and (b) PyTp-DNA complex film with $10^{-8}M$ concentration of DNA in the subphase. The scale bar in each image represents 10μm.

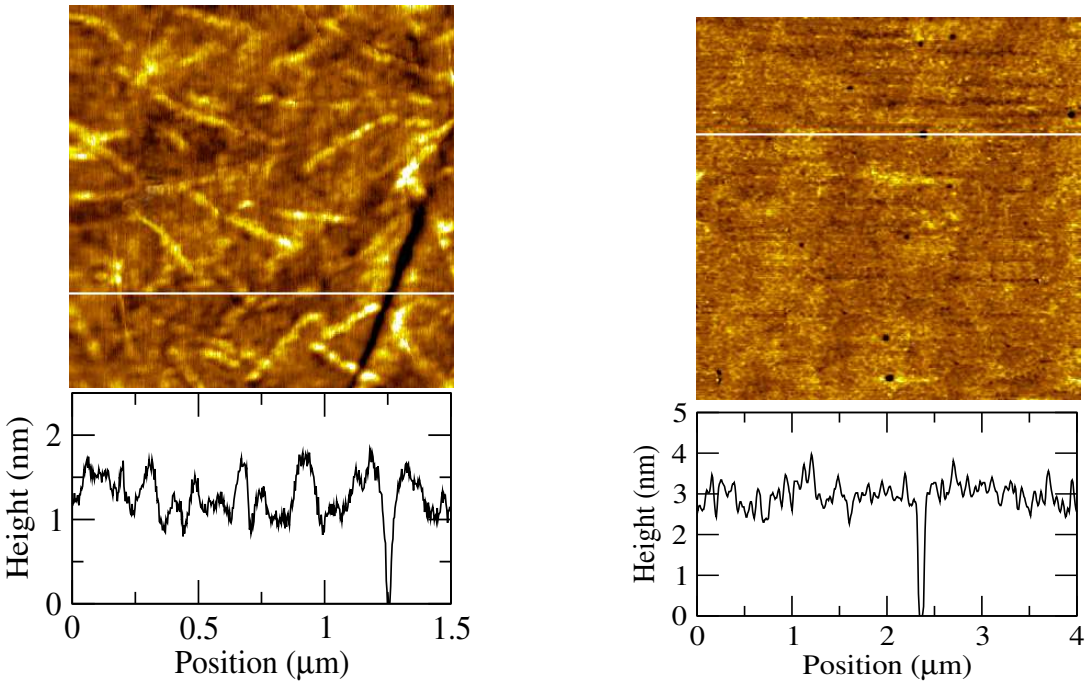

(a) π_t=5 mN/m (b) π_t=35 mN/m

Figure 3.6: AFM topography images of PyTp-DNA complex monolayer transferred at various target surface pressures (π_t) onto hydrophilic silicon substrate. The respective height profiles corresponding to the lines drawn on the images are shown below.

height of 1.4 ± 0.4 nm with reference to the substrate. The film morphology depicts heterogeneity with streak-like features. These streak-like features exhibited length in the range of 200-300 nm and width in the range of 20-30 nm. The morphology of the film transferred at a π_t of 35 mN/m (Figure 3.6(b)) was compact and homogeneous with some small voids. The film showed a height of 3 ± 0.2 nm with respect to the substrate. This height is more than the film height of pure PyTp monolayer in the edge-on configuration by nearly 1 nm.

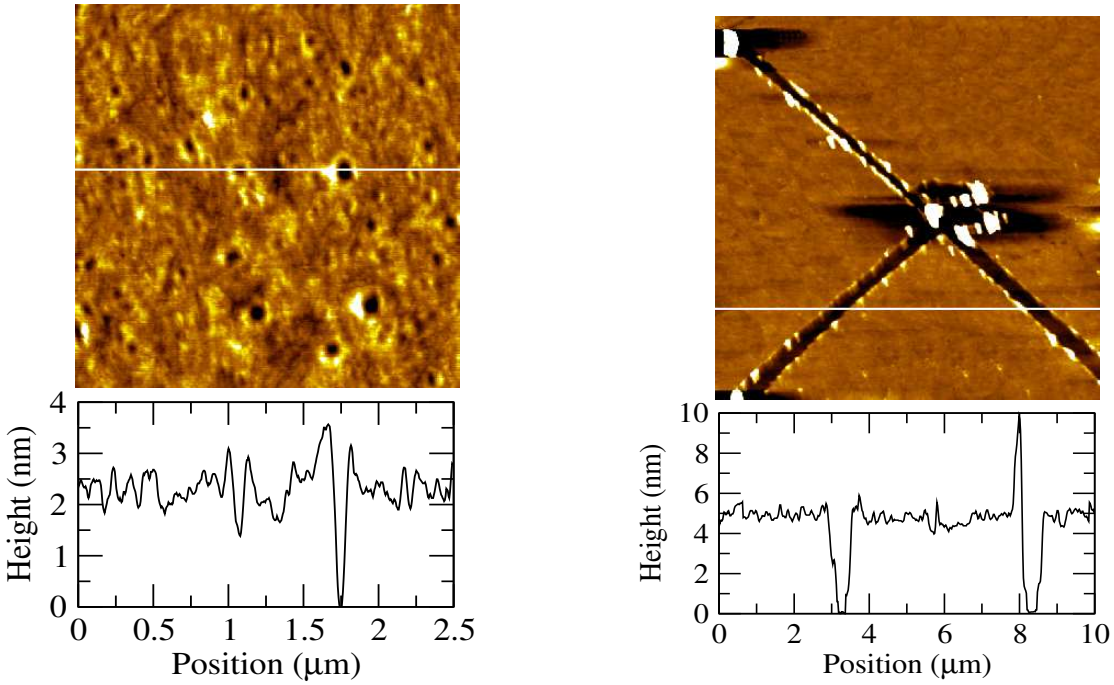

(a) (b)

Figure 3.7: AFM topography images for 2 layers of PyTp-DNA complex film transferred at 35 mN/m onto hydrophobic silicon substrate. (a) Morphology of the film surface showing roughness. (b) Scratched film to measure the thickness. The respective height profiles corresponding to the lines drawn on the images are shown below.

Figure 3.7 represents AFM topography for 2 layers of the PyTp-DNA complex LB film deposited at 35 mN/m on hydrophobic silicon substrate. As compared to the 2 layers of pure PyTp film which had regular rectangular voids [16], the morphology of PyTp-DNA complex film with 2 layers was more compact with some circular voids of different depth (Figure 3.7(a)). Some of these voids exhibited a depth of about 2 nm.

To obtain the actual film thickness, we have scratched the film using AFM tip in contact mode and then imaged the scratched region in non-contact mode using the same tip (Figure 3.7(b)). The film was scratched in different directions to obtain the thickness of the film with better reproducibility. The thickness of the film obtained from the height profile across the scratch was about 5 ± 0.5 nm. We have studied the morphology and thickness of the complex LB films transferred up to 20 layers. The AFM images of the complex films with 3, 4, 5, 12 and 20 layers are shown in Figures 3.8(a), 3.9(a), 3.10(a), 3.11(a) and 3.12(a), respectively. For all the films, the coverage was found to be good. The roughness of the film surfaces was found to increase with the number of layers. For the film with 20 layers, thread-like structures aligned in the film deposition direction were observed. These thread-like structures appeared for films with more than 5 layers and grew in number with increasing layers. The typical dimensions of these bundles were about 80 nm in width, 1.5-3.0 μm in length and 10-12 nm in height.

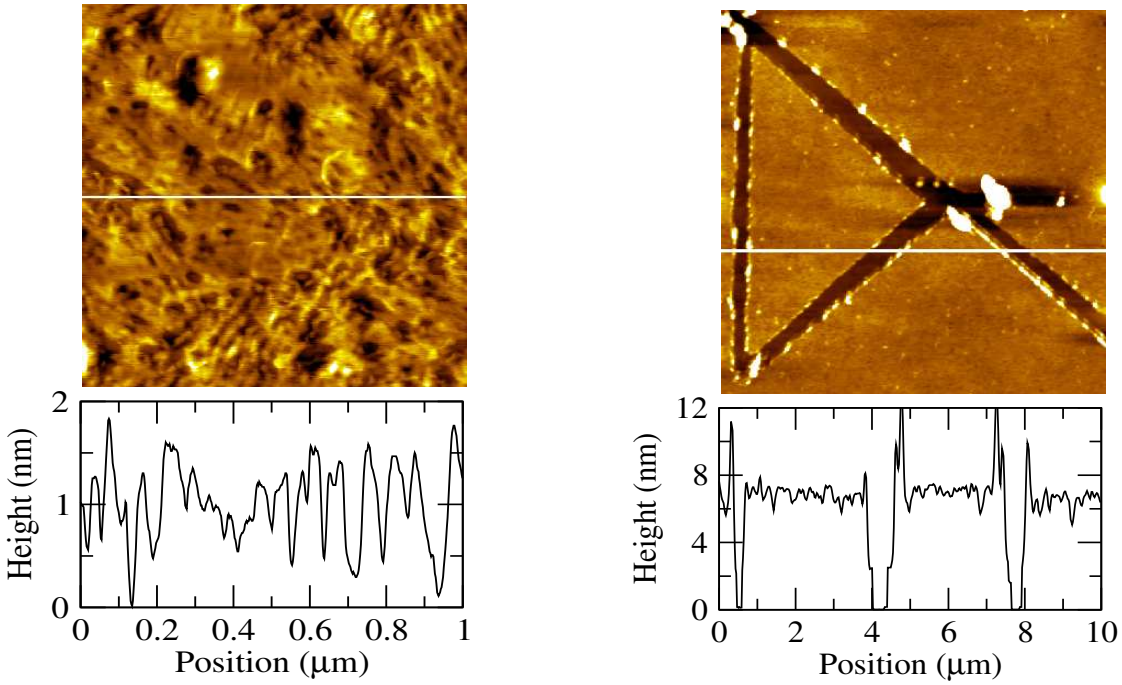

(a) (b)

Figure 3.8: AFM topography images for 3 layers of PyTp-DNA complex film transferred at 35 mN/m onto hydrophilic silicon substrate. (a) Morphology of the film surface showing roughness. (b) Scratched film to measure the thickness. The respective height profiles corresponding to the lines drawn on the images are shown below.

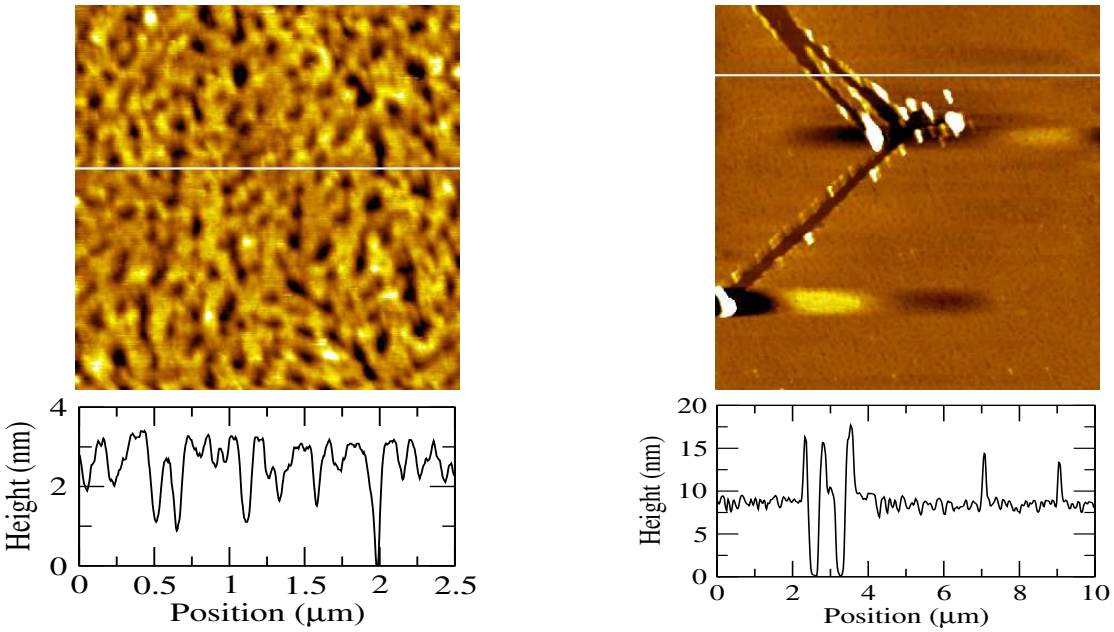

(a) (b)

Figure 3.9: AFM topography images for 4 layers of PyTp-DNA complex film transferred at 35 mN/m onto hydrophobic silicon substrate. (a) Morphology of the film surface showing roughness. (b) Scratched film showing the thickness. The respective height profiles are shown below.

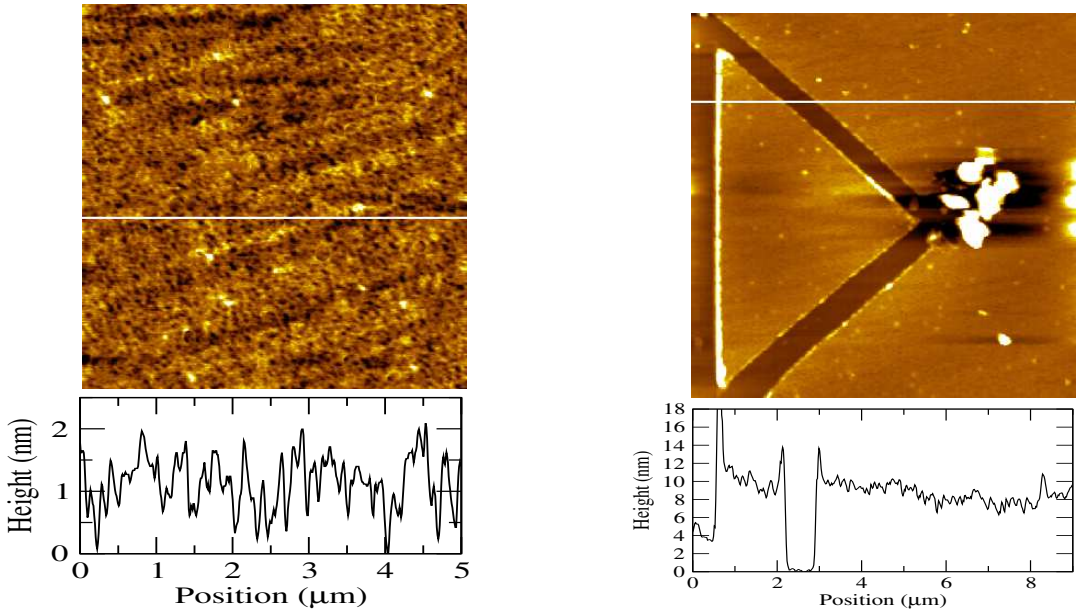

(a) (b)

Figure 3.10: AFM topography images for 5 layers of PyTp-DNA complex film transferred at 35 mN/m onto hydrophilic silicon substrate. (a) Morphology of the film surface showing roughness. (b) Scratched film showing the thickness. The respective height profiles are shown below.

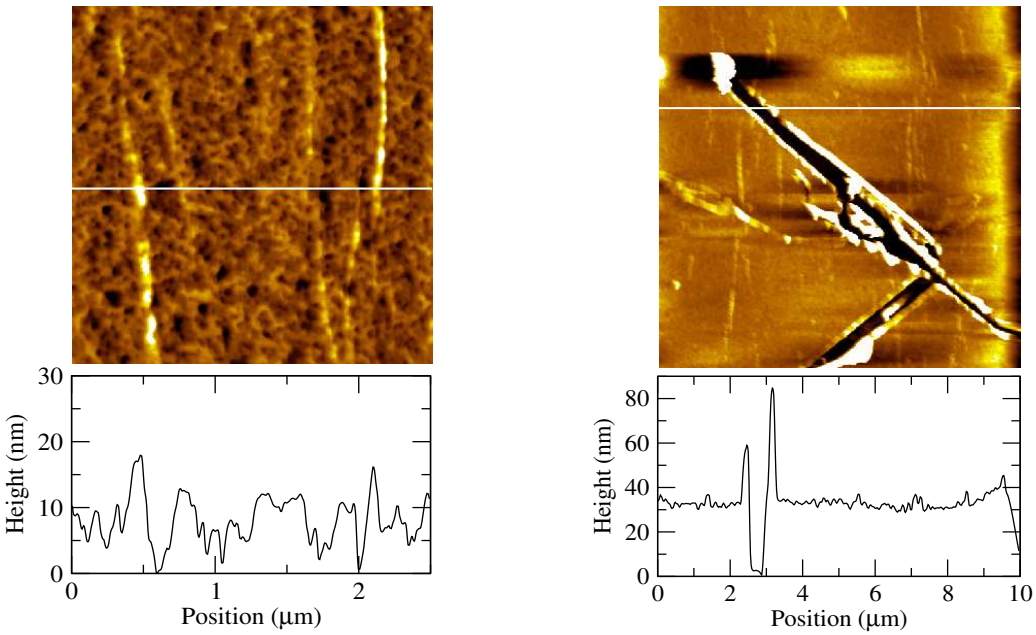

(a) (b)

Figure 3.11: AFM topography images for 12 layers of PyTp-DNA complex film transferred at 35 mN/m onto hydrophobic silicon substrate. (a) Morphology of the film surface. (b) Scratched film showing the thickness. The respective height profiles are shown below.

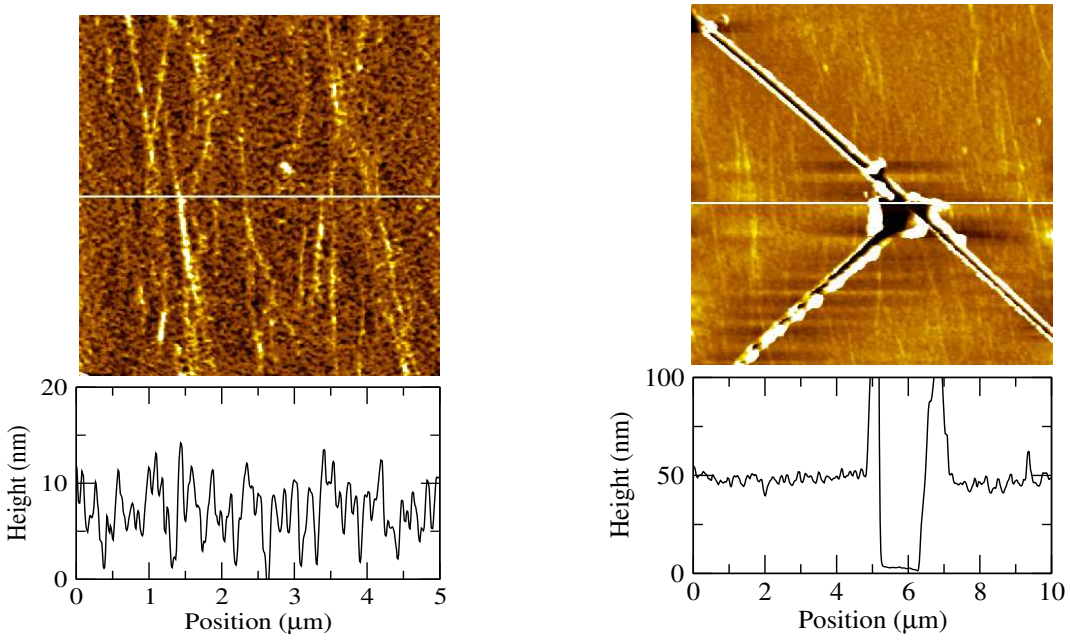

(a) (b)

Figure 3.12: AFM topography images for 20 layers of PyTp-DNA complex film transfered at 35 mN/m onto hydrophobic silicon substrate. (a) Morphology of the film surface. (b) Scratched film to measure the thickness. The respective height profiles are shown below.

To find the film thicknesses, we have scratched all the films with AFM tip. The topography of the scratched films are shown in Figures 3.8(b), 3.9(b), 3.10(b), 3.11(b) and 3.12(b) respectively. The height profiles corresponding to the lines drawn on the scratched images give the respective film thicknesses. Scratching the LB films using the AFM tip became difficult for higher layers because of large accumulation of material at the edges. Also, the tip contamination affects the correct measurement of the film height. For this reason, scratching was not performed for the films with more than 20 layers although it was possible to efficiently transfer even 50 layers.

For the pure PyTp film, it was not possible to transfer more than two layers efficiently unlike that of the PyTp-DNA complex film. The topography images of the pure PyTp film for 3 and 5 layers on hydrophilic silicon substrates are shown in Figures 3.13(a) and 3.13(b) respectively.

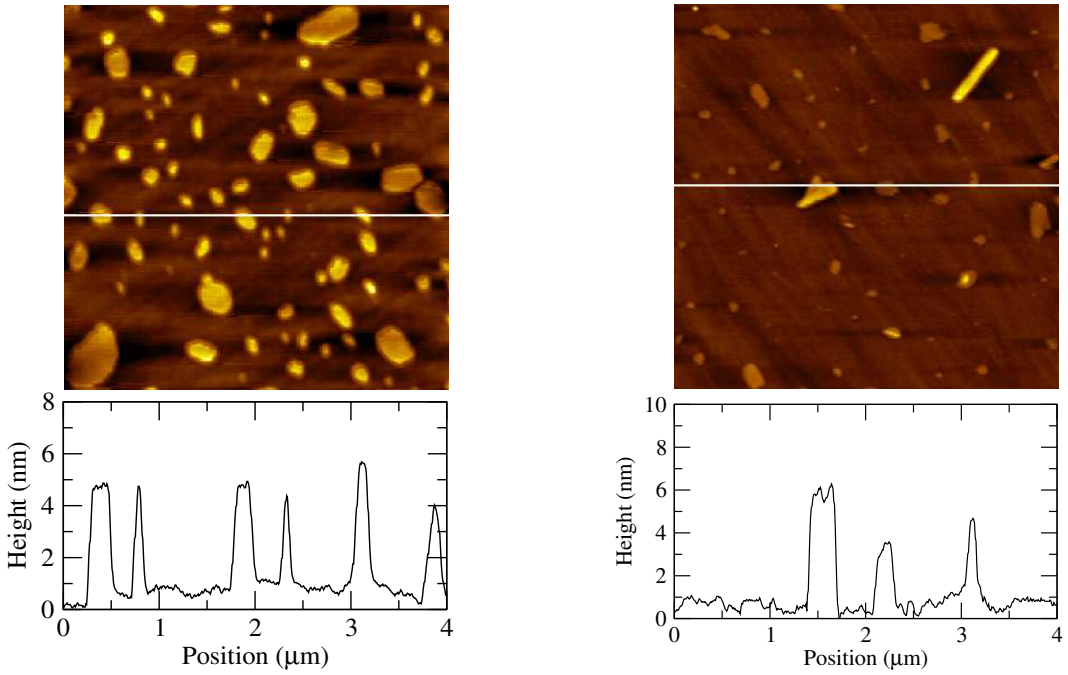

(a) 3 layers (b) 5 layers

Figure 3.13: AFM topography images for 3 and 5 layers of the pure PyTp monolayer transferred onto hydrophilic silicon substrates at 35 mN/m. The respective height profiles are shown below.

We find that the coverage is poor for the pure film with 3 layers which was even less for 5 layers. This indicates desorption of the molecules back to the subphase. Similar behavior was also observed for the transfer of pure film on a hydrophobic silicon substrate. To ensure the desorption of films back to the subphase, we have measured the transfer ratio (τ) for the number of layers (n)

of LB deposition. Figure 3.14(a) shows τ as a function of n for the LB deposition of the pure film at 35 mN/m on hydrophilic silicon substrate. We find negative transfer ratio values for more than two strokes of deposition. This provides clear evidence of desorption. In the successive strokes, we find alternate adsorption and desorption. This makes further transfer of layers of the pure film more difficult. Figure 3.14(b) shows τ as a function of n for the LB deposition of the PyTp-DNA complex film at 35 mN/m on hydrophobic silicon substrate. Unlike pure PyTp film, the PyTp-DNA complex film shows a τ value of about unity for every stroke.

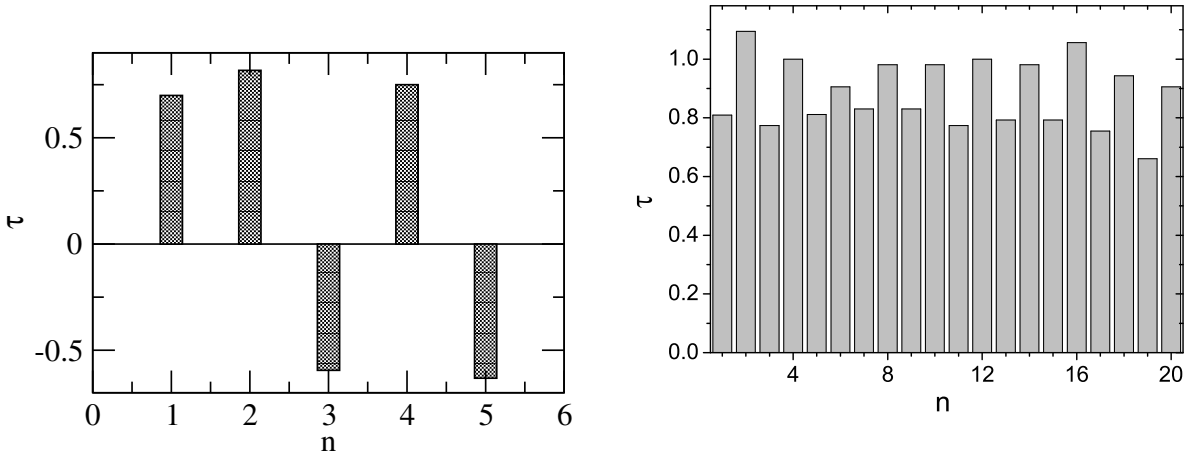

(a) (b)

Figure 3.14: Transfer ratio (τ) as a function of number of layers (n) of LB deposition at a target surface pressure of 35 mN/m for (a) pure PyTp film onto hydrophilic silicon substrate, and (b) PyTp-DNA complex film onto hydrophobic silicon substrate.

3.3.3.2 Nanoindentation

We have studied the hardness of the pure PyTp film and the PyTp-DNA complex film by performing nanoindentation using AFM in the contact mode. In a nanoindentation measurement, we obtain a force versus distance curve between the cantilever tip and the sample surface. To obtain a force curve, we first slowly lower a cantilever tip towards a surface. When the tip comes within about 1 to 10 nm of the surface, attractive van der Waal force between the atoms of the cantilever tip and those on the surface pull the cantilever down, making it snap suddenly into contact. This is called the jump-to-contact point. As we continue to lower the cantilever, it deflects as it pushes

against the surface. The cantilever tip exerts a force proportional to its deflection. Then the process reverses. The cantilever tip is pulled away from the surface. It tends to retrace the force curve obtained during its approach. At the point where the tip is about to lose contact with the surface, it instead holds on little longer. This is due to the adhesive force between the surface atoms and the tip atoms which refuses the tip to detach immediately. The more the tip is pushed into the surface, and the stickier the surface, the longer the tip will stay attached as the cantilever pulls away. Finally, the force is enough to detach the tip and it snaps back to its equilibrium position. This is called the jump-off-contact point.

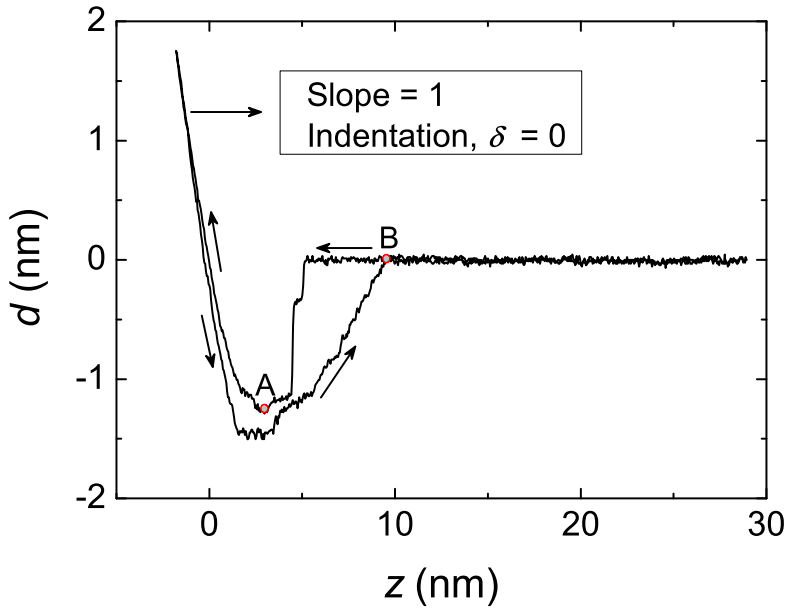

Figure 3.15: Cantilever deflection (d) versus piezo displacement (z) curves obtained at a load of 9 nN for reference silicon surface. The arrows in the figure indicate the piezo traveling direction. When the cantilever tip comes close to the surface, the attractive forces between the atoms of the tip and those on the surface pull the tip down, making it snap suddenly into contact. This is called jump-to-contact point (marked as A). As we continue to lower the cantilever, it deflects as it pushes against the surface. Then the process reverses. The cantilever is pulled away from the surface, it tends to retrace the force curve. At the point where the tip is about to lose contact with surface, the adhesion force tends to hold the tip little longer in contact with the surface. Finally, the force is enough to detach the tip and it snaps back to its equilibrium position. This is called jump-off-contact point (marked as B). Slope of the deflection curve above zero is given in the figure.

The cantilever deflection (d) versus piezo displacement (z) trace-retrace curves obtained at a load of 9 nN for a freshly cleaned silicon surface is shown in Figure 3.15. The piezo displacement gives the distance by which the tip moves with respect to the surface. Similar curves were obtained for 2 layers of pure PyTp film surface (Figure 3.16(a)) and 2 layers of PyTp-DNA complex film surface (Figure 3.16(b)), both at a load of 9 nN. The load F applied by the cantilever tip to the surface was computed from the cantilever spring constant k_c using Hooke's law,

$$F = k_c d \tag{3.2}$$

The indentation depth δ is given by,

$$\delta = z - d \tag{3.3}$$

where z is the piezo displacement and d is the deflection of the cantilever.

Due to thermal drift in the detection system, as well as to the stresses in the cantilever, the deflection of the free cantilever was not equal to zero. Therefore, it was necessary to subtract the deflection offset from all the deflection values. All the plots in Figures 3.15 and 3.16 are shown after the offset correction.

From these trace and retrace curves, the force of adhesion, jump-to-contact (point at which tip-sample contact occurs, marked A in Figures 3.15 and 3.16) and jump-off-contact (point at which tip-sample contact breaks off, marked B in Figure 3.15 and 3.16) were obtained. The amount of force just before the jump-off-contact gives a measure of the maximum tip-sample adhesion. The tip - sample adhesion for both pure and complex films was 3.75 nN which is half the value of adhesion for clean hydrophilic silicon surface (7.5 nN). From a set of ten measurements at different regions on the films, (of which Figures 3.16(a) and 3.16(b) are typical examples), the mean values of the jump-to-contact and jump-off-contact distances were obtained to be 7 ± 2 and 18 ± 5 nm respectively.

Further, we have extracted information on the hardness of the films from the deflection-displacement curves depending on the indentability of the tip into the film surface at a given load [13]. Figure 3.15 shows that the slope of the cantilever deflection vs piezo displacement to be equal to 1 because silicon is an infinitely stiff surface compared to the cantilever stiffness.

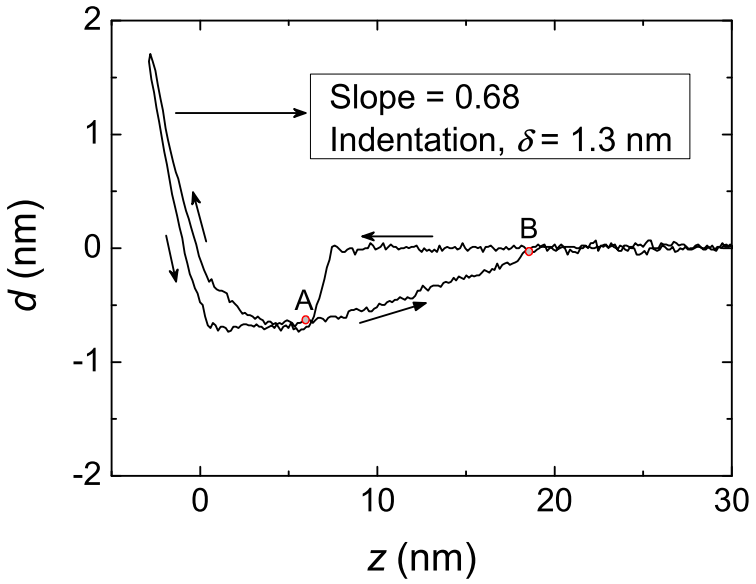

(a)

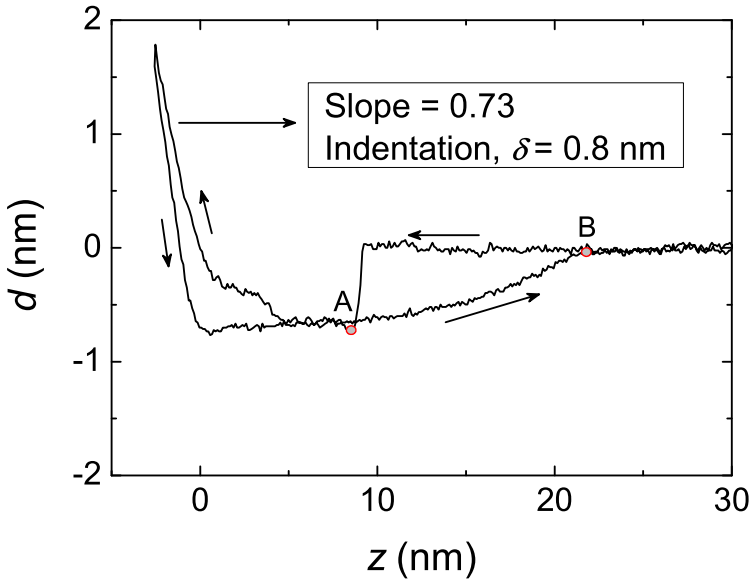

(b)

Figure 3.16: Cantilever deflection (d) versus piezo displacement (z) curves obtained at load of 9 nN for (a) 2 layers of pure PyTp film surface, and (b) 2 layers of PyTp-DNA complex film surface. The arrows in the figure indicate the piezo traveling direction. Slopes of the deflection curves above zero are given in the figure. Jump-to-contact is marked as A and Jump-off-contact is marked as B.

Hence, the tip followed the piezo displacement. On the soft film, the tip indented the film surface and the cantilever deflection was smaller than the piezo displacement, yielding a corresponding slope lower than 1. For the pure film (Figure 3.16(a)), a slope of 0.68 was obtained, whereas, for the complex film (Figure 3.16(b)), the value was 0.73 at the same load of 9 nN. The corresponding indentation depth δ of the films calculated from these curves were 1.3 nm for the pure film and 0.8 nm for the complex film at the same load. Unequal slopes during trace and retrace suggest that the deformation is inelastic and does not recover fully during retrace. Typical AFM images showing the topography of the indents formed on the pure film and complex film are shown in Figures 3.17(a) and 3.17(b) respectively. The hardness value, obtained by nanoindentation, is defined as the load divided by the projected area of the indent. However, as the indent was not uniform, it became difficult to measure the area accurately. Thus, the relative hardness can be determined qualitatively [17, 18]. Our experiments yielded the hardness value to be 3.58 MPa for the complex film and 1.79 MPa for the pure film.

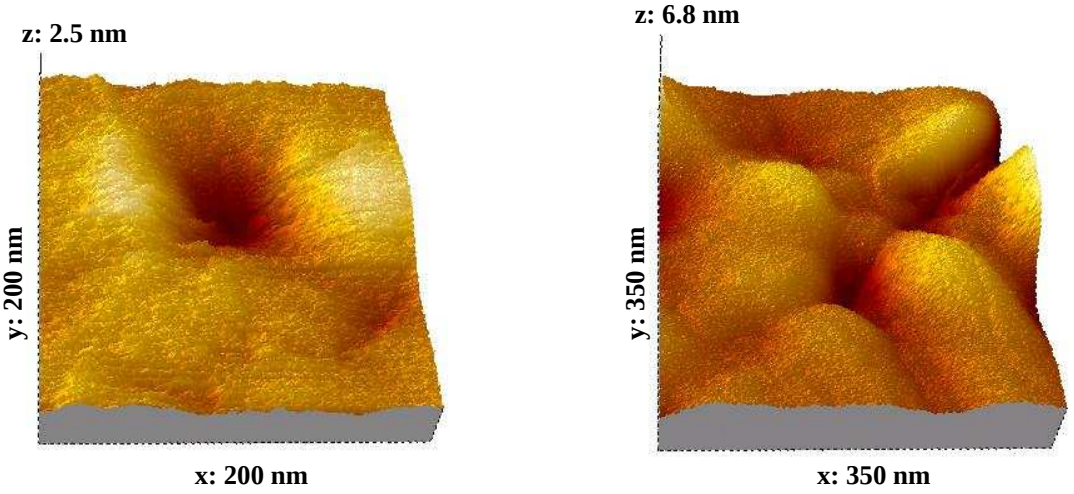

(a) (b)

Figure 3.17: The topography images of the indents formed on (a) 2 layers of pure PyTp film surface after indenting with a load of 9 nN, and (b) 2 layers of PyTp- DNA complex film surface after indenting with a load of 18 nN.

3.3.4 FTIR Spectroscopy

Transmission Fourier transform infrared (FTIR) spectroscopy was carried out to study the PyTp-DNA complex LB film transferred on hydrophilic silicon substrate. Figure 3.18 shows the FTIR absorption spectra of the pure PyTp film, and DNA in the range of 900 - 1800 cm^{-1}. The characteristic absorption peaks are shown in the figure. The FTIR absorption spectrum of PyTp-DNA complex LB film with 19 layers on hydrophilic silicon substrate is shown in Figure 3.19(a).

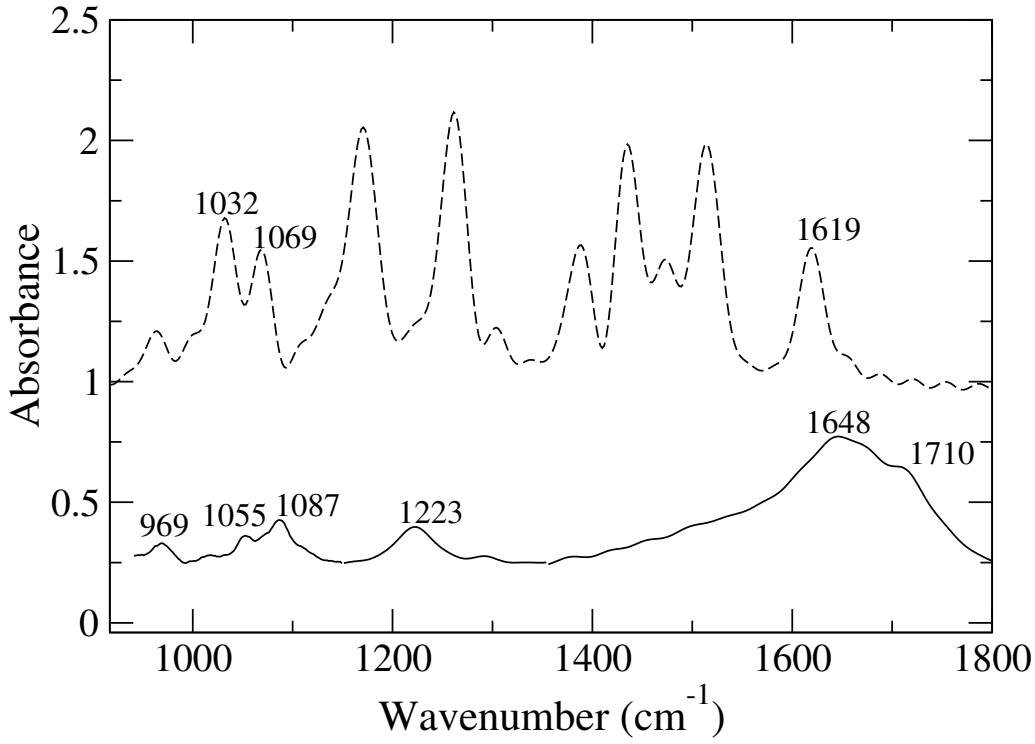

Figure 3.18: FTIR absorption spectrum for the monolayer of pure PyTp LB film on hydrophilic silicon substrate (dashed line). The solid line shows the absorption spectrum of pure DNA at a concentration of 2 mg/ml in water applied on silver chloride plate.

We find that the spectrum of the PyTp-DNA complex film possessed characteristic absorption bands of both pure PyTp and DNA with certain modifications. Figure 3.19(b) shows the FTIR spectrum of PyTp-DNA complex LB film in the range 1600 - 1720 cm^{-1} deconvoluted into individual absorption bands. We find that the peak of 1710 cm^{-1} was broadened and shifted to 1705 cm^{-1}. In addition, we find a new peak at 1684 cm^{-1} which is close to 1690 cm^{-1}. These features confirm the formation of PyTp-DNA complex.

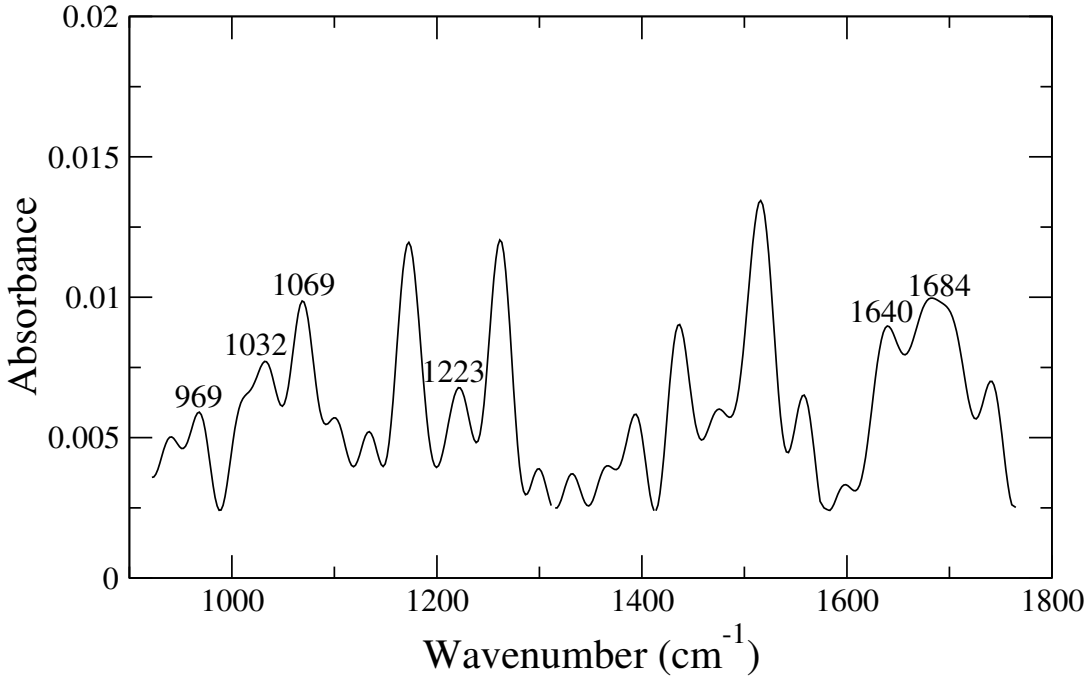

(a)

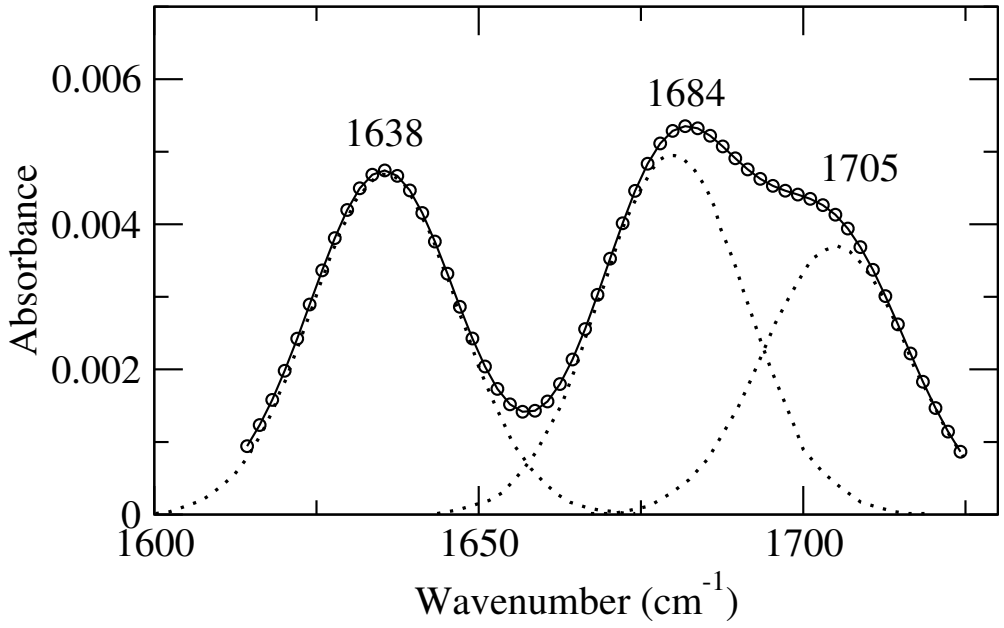

(b)

Figure 3.19: FTIR absorption spectrum of PyTp-DNA complex LB film with 19 layers: (a) In the range 900-1800 cm^{-1}. (b) The spectrum in the range 1600-1720 cm^{-1} (open circles) is deconvoluted into individual absorption bands (dotted lines).

3.4 Discussion

The surface pressure (π) - area per molecule (A_m) isotherms for the PyTp-DNA complex monolayer (Figure 3.1) showed a decrease in A_o and increase in π_c values as compared to the pure PyTp monolyer. This indicates condensation and enhanced stability of the PyTp-DNA complex monolayer [19]. This may be a consequence of the charge neutralization of the positively charged PyTp monolayer due to its complexation with negatively charged DNA. Unlike pure PyTp monolayer, the PyTp-DNA complex monolayer showed appreciable amount of hysteresis in the isotherm cycles performed between the collapsed and monolayer states. This suggests that the PyTp-DNA complex film exhibits irreversible collapse. In addition, the PyTp-DNA complex film was studied using BAM during the compression - expansion cycles. It was observed that the thread-like collapse domains did not revert back to its monolayer state on expanding the complex film (Figures 3.4(b) and 3.4(c)). This observation further confirms the irreversibility from the collapsed state to the monolayer state.

The surface pressure (π) - time (t) relaxation isotherms showed that the complex monolayer was fairly stable with time (Figure 3.2). On the basis of all these results, we suggest a stable complex formation between the DNA molecules and the cationic discotic PyTp molecules at the A-W interface. Here, the interaction is mainly electrostatic between the pyridinium group of discotic mesogen and the phosphate group of DNA which play an important role in the formation and stability of the complex film [14].

Moreover, the $|E|$ versus A_m plots (Figure 3.3) give further information about the monolayer stable phases . The maximum $|E|$ value attained by the complex monolayer (283 mN/m) was more than three times the value attained by the pure PyTp monolayer (83 mN/m). This indicates a much better packing of molecules in the complex monolayer compared to that of pure PyTp monolayer. We find a sharp change in the value of $|E|$ at an A_m of 0.95 nm^2/molecule for the complex monolayer indicating a phase transformation. The phase above an A_m of 0.95 nm^2/molecule has much lower value of $|E|$ (25 mN/m), whereas, the phase below this A_m has much higher value of $|E|$ (283 mN/m). The isotherm (Figure 3.1) also showed a phase transformation at an A_m of 0.95 nm^2/molecule. The A_o value was 1.9 nm^2/molecule for the first transformation

and 0.9 nm^2/molecule for the second transformation. Comparing these A_o values with the molecular dimension (shown in Chapter 2) and on the basis of the $|E|$ values obtained, we suggest that the PyTp-DNA complex film undergoes a phase transformation from an expanded phase to a condensed phase.

The AFM topography images of the PyTp-DNA complex monolayer (Figure 3.6) showed a height of 1.4 ± 0.4 nm for the film transferred at the expanded phase and 3.0 ± 0.2 nm for the film transferred at the condensed phase. Comparing with the molecular dimension (Chapter2), we find that the height of 1.4 ± 0.4 nm lies in between the values expected for the face-on and edge-on configurations of molecules in the film, whereas, the height of 3.0 ± 0.2 nm is well suited for the molecules in an edge-on configuration. Therefore, we infer that the complex monolayer undergoes a phase transition in the edge-on configuration from an expanded phase to a condensed phase. Unlike the pure PyTp film, the face-on configuration was suppressed for the PyTp-DNA complex film. Further, the expanded phase can be interpreted as loosely packed molecules in the edge-on configuration, whereas, the condensed phase can be interpreted as compactly packed molecules in the edge-on configuration [14]. On the basis of all these results, we schematically represent the configuration of molecules in the expanded phase and condensed phase of the complex film at the A-W interface in Figure 3.20.

In addition, the AFM images revealed many interesting features for the complex film. For the monolayer film of the complex at 5 mN/m, several streak-like features were observed (Figure 3.6(a)). This may be due to the DNA strands complexed with the PyTp molecules in the film with a loosely packed configuration. An extra thickness of 1 nm was observed for the complex monolayer film as compared with the pure film at 35 mN/m (Figure 3.6(b)). This can be attributed to the presence of DNA in the film, but the value is markedly smaller than the geometrical size of the cylindrical DNA (diameter 2 nm). Wu et. al. reported lipid-DNA LB monolayer film to be thicker than the pure lipid film by about 0.9 nm employing neutron and X-ray reflectivity techniques [20]. Kago et.al. confirmed by direct in situ X-ray reflectivity technique that the structure and conformation of the DNA molecule in the lipid-DNA complex deposited on solid substrate were very different from its conformation at the A-W interface. They found the thickness of the

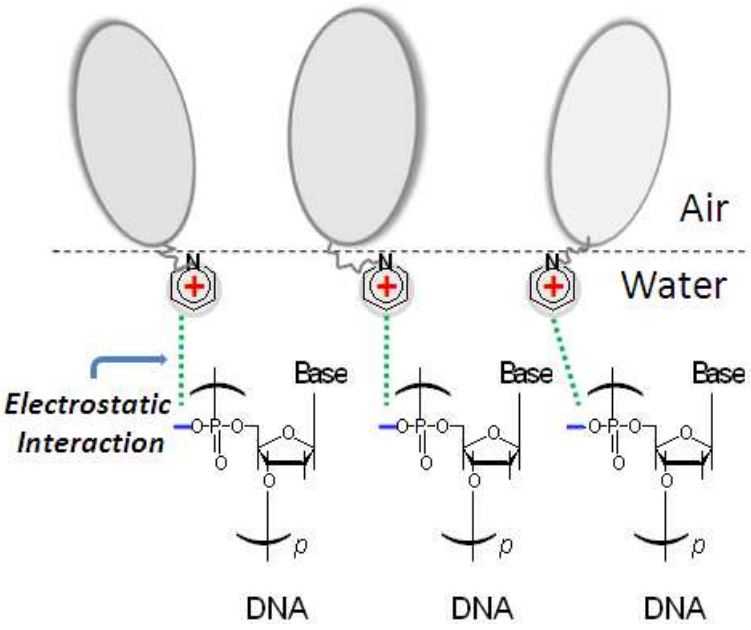

(a)

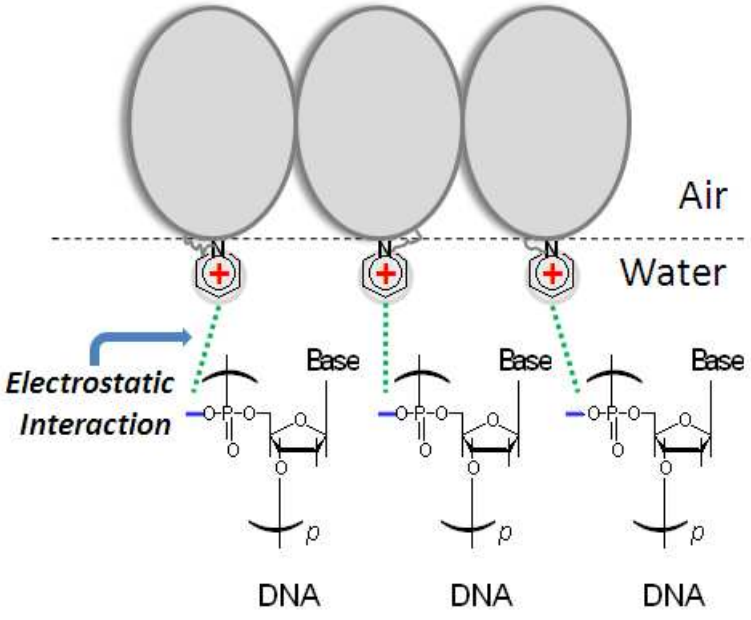

(b)

Figure 3.20: Schematic representation of the PyTp-DNA complex monolayer in the edge-on configuration formed at the air-water interface by electrostatic interaction. (a) Loosely packed molecules at A_0 value of 1.9 nm^2/molecule. (b) Compactly packed molecules at A_0 value of 0.9 nm^2/molecule.

DNA layer in the lipid-DNA complex film at the A-W interface to be about 2.5 to 2.8 nm, which is comparable to the diameter of DNA molecule. When those films were deposited on solid substrates, the thickness decreased to about 1.1 nm, which is small compared to the diameter of the DNA molecule [21]. The extra thickness of 1 nm, which we find for the complex film, is in good agreement with these reports confirming the PyTp-DNA complex formation.

For the complex film with two layers (Figure 3.7(a)), voids with different depths were observed. These might have developed in the film deposition process due to the drainage or evaporation of the entrapped water molecules within the films. We have studied the morphology of the complex films for layers upto 20. We find that the roughness of the film surface increases with the increase in the number of layers of film deposition. The surface topography of the films might not always correspond to the actual film height. For this reason, we have found the actual film thicknesses by scratching the films with AFM tip. For the complex film with 20 layers (Figure 3.12(a)), thick DNA bundles aligned in the film deposition direction were clearly observed. This may be due to the strong Π-Π stacking interaction between the discotic cores bringing multiple DNA molecules together to form these thread-like bundles [22]. The notable variation in the dimensions of these DNA bundles suggests partial coiling up or self folding of the DNA molecules [1]. Possible explanations for the alignment of these structures in the film deposition direction may be parallel alignment of the DNA strands at the A-W interface and an effect created as a result of the receding meniscus force during the transfer process. Our observation is consistent with the reports on the orientation of DNA strands along the dipping direction of LB films [1, 23].

Interestingly, stable multilayers with even 50 layers or more can be efficiently formed for the PyTp-DNA complex film. On the other hand, the pure PyTp film can only form two layers with good efficiency on a substrate. For more than 2 layers, negative transfer ratio (τ) was observed (Figure 3.14(a)) indicating desorption of the film back to the subphase. Whereas, for the complex film, τ value was about unity for every deposition cycle (Figure 3.14(b)). We believe that it is not only the ionic-ionic interaction but the packing of the PyTp molecules and DNA molecules that brings the stability. This is indicated by the decrease in the limiting area and increase in surface pressure of the complex film as compared with the pure PyTp film. LB film deposition is a physical

adsorption process and it is sensitive to the packing of molecules in a film and its stability [24]. In addition, the τ values for the complex film deposition were found to vary for the upstroke and downstroke in every deposition cycle. In literature, similar behavior is reported for charged Langmuir monolayer deposition [25]. This may be attributed to the fact that the contact angle between the substrate and the subphase changes for the up and down strokes causing a difference in τ. Further details on the factors affecting the deposition of a charged Langmuir monolayer are discussed in Chapter 7.

The cantilever deflection (d) versus piezo displacement (z) curves obtained in the nanoindentation measurements provide further insight into the system (Figure 3.16). A difference in the tip-sample adhesion was observed between the reference silicon substrate and film surface. Adhesion values of 7.5 and 3.75 nN were obtained for the reference silicon surface and sample covered surface respectively. It is known in literature that silicon is a high-energy surface and is covered with a thin layer ($\sim$ 2.5 nm) of native SiO_2 [26]. Under ambient conditions, SiO_2 readily adsorbs water, so that the outermost layer of a SiO_2 surface is usually covered with a high density of hydroxyl groups, approximately one silanol group per 0.6 nm^2. The surfaces of the silicon tips as well as the reference silicon substrate were expected to be covered with OH groups and thus behaved as hydrophilic surfaces [27]. On the other hand, both the PyTp and PyTp-DNA complex film surfaces were hydrophobic. It appears quite reasonable that the adhesion between a hydrophilic tip and a hydrophobic sample surface is less than that for a hydrophilic reference surface [28, 29]. Additionally, the retraction curves suggest that the adhesive interaction between the tip and the film surface did not allow the tip to break away from the surface abruptly, but produced a more gradual response.

From the nanoindentation studies, less indentation on the complex film surface than that on the pure film surface for a given load suggests the complex film to be harder than the pure film. A qualitative measurement of hardness showed that the PyTp-DNA complex film is about two times as hard as the pure PyTp film [14]. The hardness of films can be important in surface mechanical property studies of materials and has great potential in understanding the role of interface in defect production [30].

The FTIR studies provide evidence for the presence of DNA in the complex film. Also, information on the type of interaction between the DNA and PyTp molecules can be obtained. It is known in literature that, at high relative humidity (>75%) DNA molecules are regular double helix having a 1710 cm^{-1} absorption band of C=O stretching vibrations of stacked base pairs [8]. The 1710 cm^{-1} band disappears when the regular double helix is destroyed (for example when the DNA film is dried), and a new 1690 cm^{-1} band attributed to carbonylic group vibrations of unstacked bases appears. The 1648 cm^{-1} absorption band is attributed to the C=N and C=C stretching in the aromatic bases of DNA. The 1223 cm^{-1} absorption band (attributed to PO_2^- antisymmetric stretching vibrations) and 970 cm^{-1} absorption band (attributed to strongly coupled sugar phosphodiester vibrations) are standard markers of the B-form conformation of DNA [10, 31]. The absorption bands at 1710 cm^{-1}, 1648 cm^{-1}, 1223 cm^{-1}, and 969 cm^{-1} in Figure 3.18 ensure the regular double helix structure of pure DNA. We find that the FTIR spectrum of the complex film contains the absorption bands of DNA (Figure 3.19). This confirms the transfer of DNA molecules from the A-W to the A-S interface by LB process. Judging from the absorption band at 1223 cm^{-1} in the PyTp-DNA complex FTIR spectrum, we infer that DNA maintained the B-form conformation. The shifts and broadening of the peaks in the absorption spectrum of the complex film indicate that the base pair stacking in DNA molecules were partially disturbed due to complexation with the PyTp molecules. This may be caused by the replacement of intramolecular nucleic base-base hydrogen bonds by intermolecular nucleic base-PyTp hydrogen bonds. The positively charged pyridinium group of PyTp molecule interact electrostatically with the negatively charged phosphate (PO_2^-) groups of the DNA backbone forming stable bonds in the process of PyTp-DNA complex formation. These interactions provide stability to the multilayer films of the complex.

The most interesting feature of the system is that the DNA complexation facilitated the film deposition of several tens of layers with high transfer efficiency. The ability to transfer several layers gives an excellent scope for device applications like field-effect transistors [32]. Moreover, the immobilization of nucleic acids onto solid supports by LB technique is a useful approach in designing the nucleic acid based biosensors [8, 9].

3.5 Conclusions

We have shown the supramolecular complexation between DNA and a cationic discotic mesogen (PyTp) at the A-W interface. The PyTp-DNA complex was formed primarily due to the electrostatic interaction between the pyridinium group of the triphenylene molecule and the phosphate group of DNA. The formation of DNA complex has enhanced the transfer efficiency over several tens of layers. AFM studies on the LB films showed that the PyTp-DNA complex monolayer was thicker than the pure PyTp monolayer by about 1 nm. This thickness is reasonable for a DNA layer in a dried state and is comparable to the reported values using neutron and X-ray reflectometry. The nanoindentation studies using AFM showed that the PyTp-DNA complex film was about two times harder than the pure PyTp film. FTIR spectroscopy suggests that the DNA double helical structure gets partially disturbed due to the complexation with the PyTp molecules.

The ability of the PyTp-DNA complex to form multilayers on a substrate has potential application in the fabrication of devices like thin film transistors and nucleic acid-based biosensors. In the long-term and successful performance of devices, the mechanical stability of the materials play significant role. In this chapter, we have presented only a qualitative measure of hardness for the films. A more detailed and quantitative analysis of the mechanical properties are described in the next chapter.

Bibliography

[1] A. Bhaumik, M. Ramakanth, L. K. Brar, A. K. Raychaudhuri, F. Rondelez, and D. Chatterji, *Langmuir* **20**, 5891 (2004).

[2] J. O. Radler, I. Koltover, T. Salditt, and C. R. Safinya, *Science* **275**, 810 (1997).

[3] D. Putnam, *Nature Materials* **5**, 439 (2006).

[4] M. Guillot-Nieckowski, D. Joester, M. Stohr, M. Losson, M. Adrian, B. Wagner, M. Kansy, H. Heinzelmann, R. Pugin, F. Deiderich, and J. L. Gallani, *Langmuir* **23**, 737 (2007).

[5] M. P. W. Frances, L. R. Dorothy, and B. B. Marcel, *Biochemistry* **35**, 5756 (1996).

[6] M. Sastry, V. Ramakrishnan, M. Pattarkine, A. Gole, and K. N. Ganesh, *Langmuir* **16**, 9142 (2000).

[7] D. D. Lasic and N. S. Templeton, *Advanced Drug Delivery Reviews* **20**, 221 (1996).

[8] G. B. Sukhorukov, M. M. Montrel, A. I. Petrov, L. I. Shabarchina, and B. I. Sukhorukov, *Biosensors and Bioelectronics* **11**, 913 (1996).

[9] J. J. Gooding and G. C. King, *J. Mater. Chem.* **15**, 4876 (2005).

[10] L. Cui, J. Miao, and L. Zhu, *Macromolecules* **39**, 2536 (2006).

[11] D. Tranchida, S. Piccarolo, and M. Soliman, *Macromolecules* **39**, 4547 (2006).

[12] Sandeep Kumar and Santanu Kumar Pal, *Tetrahedron Letters* **46**, 4127 (2005).

[13] B. Du, O. K. C. Tsui, Q. Zhang, and T. He, *Langmuir* **17**, 3286 (2001).

[14] Alpana Nayak and K. A. Suresh, *J. Phys. Chem. B* **112**, 2930 (2008).

[15] G. Roberts, *Langmuir-Blodgett Films*, Plenum Press: New York, 1990.

[16] Alpana Nayak, K. A. Suresh, Santanu Kumar Pal, and Sandeep Kumar, *J. Phys. Chem. B* **111**, 11157 (2007).

[17] B. Bhushan, A. V. Kulkarni, V. N. Koinkar, M. Boehm, L. Odoni, C. Martelet, and M. Belin, *Langmuir* **11**, 3189 (1995).

[18] D. H. Gracias and G. A. Somorjai, *Macromolecules* **31**, 1269 (1998).

[19] V. Matti, J.Saily, S. J. Ryhanen, J. M. Holopainen, S. Borocci, G. Mancini, and P. K. J. Kinnunen, *Biophysical Journal* **81**, 2135 (2001).

[20] J. C. Wu, T. L. Lin, U. S. Jeng, H. Y. Lee, and T. Gutberlet, *Physica B* **385**, 841 (2006).

[21] K. Kago, H. Matsuoka, R. Yoshitome, H. Yamaoka, K. Ijiro, and M. Shimomura, *Langmuir* **15**, 5193 (1999).

[22] X. Chen, J. Wang, and M. Liu, *J. Colloid Interface Sci.* **287**, 185 (2005).

[23] Y. Okahata, T. Kobayashi, and K. Tanaka, *Langmuir* **12**, 1326 (1996).

[24] D. K. Schwartz, *Surface Science Reports* **27**, 241 (1997).

[25] M. Elena Diaz and R. L. Cerro, *Thin Solid Films* **460**, 274 (2004).

[26] T. Nguyen, W. E. Byrd, and D. Bentz, *J. Adhes.* **48**, 169 (1995).

[27] D. Raghavan, X. Gu, T. Nguyen, M. VanLandingham, and A. Karim, *Macromolecules* **33**, 2573 (2000).

[28] T. Akihiro, M. Sasaki, K. Hane, and S. Okuma, *Sensors and Actuators A* **40**, 71 (1994).

[29] M. Binggeli and C. M. Mate, *Appl. Phys. Lett.* **65**, 415 (1994).

[30] R. C. Thomas, J. E. Houston, T. A. Michalske, and R. M. Crooks, *Science* **259**, 1883 (1993).

[31] C. S. Braun, G. S. Jas, S. Choosakoonkriang, G. S. Koe, and J. G. Smith, *Biophysical Journal* **84**, 1114 (2003).

[32] W. Pisula *et al.*, *Adv. Mater.* **17**, 684 (2005).